Materials Advances

ROYAL SOCIETY OF CHEMISTRY

PAPER

View Article Online
View Journal | View Issue

Cite this: *Mater. Adv.*, 2025, **6**, 184

Green synthesis and physicochemical characterization of an eco-friendly zero-valent iron biochar based on *Coula edulis* shell and morinda bark extracts using response surface analysis

C. A. Ntinkam Simo,[a] J. M. Dika[a] and C. M. Kede*[ab]

Received 14th July 2024,
Accepted 11th August 2024

DOI: 10.1039/d4ma00714j

rsc.li/materials-advances

In the present study, two biochars obtained from waste agricultural residue were chemically activated with H_2SO_4 (HN/AC) and impregnated with zero-valent iron using morinda stem bark extract as a reducing agent (HN/AC/Fe°). The central composite design (CCD) of response surface methodology with three replicated centre points was used to optimize the operating conditions for the production of both biochars. The precursor and the prepared biochars were characterized *via* FTIR, TGA, SEM, BET and XRD analyses, and their efficiency was tested for the elimination of malachite green. The optimum synthesis conditions for HN/AC (1 N sulphuric acid, 10 g *Coula edulis* and 30 min) and HN/AC/Fe° (0.075 M iron concentration, 6 g morinda and 60 min) permitted us to obtain specific surface areas of 178.136 and 361.70 $m^2\ g^{-1}$, respectively. The biochar HN/AC/Fe° presented a microstructure, which was more amorphous and more porous than HN/AC. HN/AC/Fe° demonstrated an elimination rate of 97.08% for malachite green. These results show that response surface methodology is an outstanding and useful tool for the optimal synthesis of biochar engineered using zero-valent iron and morinda stem bark extract.

1. Introduction

Agricultural activities extensively generate by-products, which can seriously pollute the environment when allowed to decompose. They generally have a very low rate of use and cannot be applied as a food resource for animals. Nonetheless, these wastes are generally disposed of in unconventional ways, causing serious environmental pollution and the loss of several bioenergy resources.[1,2] Researchers have developed several strategies to reduce the quantity of agricultural wastes present in the environment and, particularly, to give them a market value.[3–6] Among these ideas is to use such as the transformation of these wastes into adsorbents intended for the treatment of aqueous effluents using adsorption techniques. The simplicity of use, flexible design, low cost and high efficiency of such materials facilitates their effective application in the elimination of various water pollutants, such as heavy metals and dyes.[7,8] Previous studies have reported on activated carbon preparation using *Coula edulis* nut shells.[9] Nevertheless, the synthesis of activated carbon from agricultural waste is expensive and sometimes requires harmful chemicals. This has led to a growing interest in the synthesis of eco-friendly adsorbents.

Biochar, a stable carbon-rich powder-form adsorbent, is generally derived from heating agricultural and forestry waste at moderate temperatures (<700 °C) under a limited oxygen supply.[10] Biochars possess good properties, such as eco-friendliness, abundance of inorganic mineral species and functional groups, a high surface area, high adsorption capacity and micro- and/or mesoporous structures.[11,12] These properties enable biochar to be used for several years as a carbon sink in soil, soil conditioner to improve soil fertility when applied to soil and for the treatment of water contaminated with various organic and inorganic contaminants.[13,14] However, biochars have some limitations in the effective absorption of high concentrations of contaminants since the contents of their surface functional groups are insufficient.[15] According to certain studies,[16,17] the effectiveness of these adsorbents can be increased by the activation or modification of the surface functional groups, porous structure and specific surface area. The introduction of iron species onto biochar has proven to be an effective means to enhance the biochar performance. Nano zero-valent iron (nZVI) possesses a nanoscale particle size, large surface area, and reductive nature. Despite these apparent benefits, nZVI's applicability is difficult due to its oxidative nature and aggregation potential.[18] Thus, if composited with biochar, nZVI can become stabilized, inevitably resulting in

[a] *Department of Chemistry, Faculty of Science, University of Douala, P. O. Box 24175, Douala, Cameroon. E-mail: meleack@yahoo.fr*
[b] *Department of Process Engineering National Higher Polytechnic School of Douala, University of Douala, P. O. Box 2701, Douala, Cameroon*

its lower agglomeration and more viable applicability.[11,18,19] The synthesis of nZVI can be done by chemical and physical methods, including top-down and bottom-up methods.[20] Nevertheless, these methods generally have limitations, such as high production cost, the use of specific and expensive equipment, high energy consumption, the production of flammable gas (hydrogen), and the need for the utilization of chemical materials that may be toxic, such as stabilizing and dispersing agents, like sodium borohydride ($NaBH_4$) and organic solvents.[20] Consequently, the development of simple, inexpensive, non-dangerous, bio-based, and eco-friendly synthesis methods for nZVI is required. Lately, a green chemistry method has been developed by researchers for the synthesis of nZVI. This method makes use of plant extracts, such as green tea leaves,[21] eucalyptus leaves,[22] and mint leaves.[23] Due to their antioxidant contents, such as polyphenols, reducing sugars, nitrogenous bases, and amino acids, plant extracts can be used as reducing and capping agents.[24,25] Previous researches showed that nZVI prepared using green tea extract could remediate contaminated water efficiently. For instance, one study[26] prepared bentonite-supported nZVI using green tea extract as a reductant to remove Cr(VI) in solution. The results showed that the adsorption capacity reached 66 mg g^{-1} at pH 5, and 0.05 M ionic strength. Another study[27] used green tea extract to synthesize nZVI, and the suspension could remove 69.4% of Cr(VI) in aqueous solution within 2 days when the initial Cr(VI) concentration was 50 mg L^{-1}, Fe(tot) was 160 mg L^{-1}, pH value was 4.58 and temperature was 295 K, respectively. Yet another study[28] prepared nZVI suspensions using green tea extract (GT-nZVI), and reported a maximum reduction of 10.7 μmol Cr(VI) per mL of GT-nZVI at pH 2.5. Green-synthesized nZVI has thus shown good performance for the removal of contaminants in various studies; however, there are few reports using a green synthesis method to synthesize iron-based metallic systems.

Consequently, the present study aimed to perform the synthesis and characterization of an activated biochar and nZVI biochar making use of *Coula edulis* nut shell and morinda stem bark extract as reducing agents *via* the central composite design of the response surface methodology.

2. Experimental

2.1. Materials

All the reagents and solvents were acquired from Merck and Sigma Aldrich and used as received, including iron(III) chloride hexahydrate ($FeCl_3{\cdot}6H_2O$; 99%), sulphuric acid (98%), and ethanol (98%).

2.2. Precursor material location and conditioning

The *Coula edulis* nut shell used in this work was collected from a small village on the national road number 7 called Bivouba (latitude: 3°20.750′N, longitude: 10°5.890′E) in the southern region of Cameroon. The sample was ground mechanically and sieved over a 0.125 mm mesh. The sieved sample was then stored in a jar.

2.3. Collection of morinda stem bark extract

Morinda lucida fresh stem bark was collected from Bwega Pongo-Dibombari, Littoral region, Cameroon. After collection, it was washed, dried, and mechanically ground. The extract was obtained by boiling a given mass of the ground morinda with 100 mL distilled water for 10 min, then allowed to cool, before filtering with Whatman's no. 1 filter paper three times. The extract thus obtained had a brown colour.

2.4. Experimental design

The effects of the variables in the biochars preparation were studied using the response methodology, applying a central composite design; for instance, the different variables used for the precursor activation and impregnation. Also, the effect of the interactions between the various factors that control the process was evaluated using the central composite design, which allowed reducing the number of error attempts.[29] In this work, the variables whose effect was observed immediately in the activation process were the concentration of the oxidizing agent (x_1) ranging between 1 and 5 N, mass of adsorbent (x_2) between 10 and 20 g, and activation time (x_3) between 30 and 60 min. For the impregnation process, the variables observed were iron(III) chloride hexahydrate concentration (x'_1) ranging between 0.05 and 0.1 M, morinda mass (x'_2) varying between 2 and 10 g, and stirring time (x'_3) varying between 1 and 3 h. The choice of these different factors were inspired by previous works in the literature.[10,11,15,30–32] In practice, the total number of tests (N) performed for a composite design consists of a test number of the factorial plane 2^k, a test number of the star plane ($2k$), and a central test number (n_c usually ≥ 2), which is used to determine the experimental errors and verify the reliability of the results; where k is the number of variant factors. Eqn (1) was used to determine the number of tests to be performed.[33]

$$N = 2^k + 2k + n_c = 2^3 + 2(3) + 6 = 20 \quad (1)$$

Design expert version 13 software was used to carry out the experiments. These experiments were done randomly to minimize uncontrolled factors' effects. The empirical model used was developed using the expected response for each experiment. The empirical model used the second-order polynomial equation, eqn (2), to correlate the response to the three factors varied here[34].[6]

$$Y = b_0 + \sum_{i=1}^{n} b_i x_i + \sum_{n=1}^{n} b_{ii} x_i^2 + \sum_{i=1}^{n-1} \sum_{j=i+1}^{n} b_{ij} x_i x_j \quad (2)$$

where Y is the predicted response, b_0 is the coefficient constant, b_i is the linear term coefficient, b_{ii} is the interaction coefficient, b_{ij} is the quadratic term coefficient, and x_i and x_j are the parameters of the coded values considered.

The amounts of iodine (IN) and methylene blue (MB) adsorbed (mg g^{-1}) were the expected responses, which could be obtained from eqn (3) and (4) respectively.[31]

$$\mathrm{IN} = \frac{C_0 - C_n \cdot \frac{V_n}{2V}}{m} M V_{ad} \quad (3)$$

where C_0 is the initial concentration of iodine (I_2), C_n is the sodium thiosulfate concentration, V_n is the volume of $Na_2S_2O_3 \cdot 5H_2O$ used for I_2 standardization, V_{ad} is the volume of iodine used during adsorption, V is the volume of iodine used for the titration, M is the molar mass of I_2, and m the mass in g of the adsorbent used.

$$\mathrm{MB} = \frac{C_0 - C_e}{m} \cdot V \quad (4)$$

where m is the adsorbent mass, V is the volume of the solution, and C_0 (mg L^{-1}) and C_e (mg L^{-1}) are the initial and equilibrium concentrations of methylene blue, respectively.

Tables 1 and 2 show the different considered experimental variables in this work.

2.5. Preparation of the adsorbents

The decision to perform the conversion of *Coula edulis* nut shells after activation and impregnation into biochar was made because of the limitations this nut shell presented in previous work.[35]

2.5.1. Activation of the hazelnut shell. Making use of one of the matrices generated by the experimental design process, 10 g of raw hazelnut shell was weighed into a 250 mL beaker and 50 mL of 1 N H_2SO_4 solution was added and the solution was placed on a magnetic stirrer. The solution was energetically mixed for 30 min. Distilled water was used to wash the obtained activated hazelnut shell so as to guarantee the supernatant could attain neutrality (pH 7), and subsequently the hazelnut shell was dried in an oven at 80 °C for 8 h. Thereafter, the activated hazelnut shells were further heated at 200 °C under oxygen-limiting conditions in a muffle furnace. The furnace was heated at a rate of 5 °C per min and held at the peak temperature for 2 h before cooling to room temperature. The obtained biochar was named HN/AC (Fig. 1). The same procedure was repeated for the other samples as generated by the experimental design (DOE). The activated hazelnut shell sample with the best response was selected for impregnation with zero-valent iron.

2.5.2. Impregnation of the activated hazelnut shell. Using one of the matrices generated by the experimental design, 100 mL of an $FeCL_3 \cdot 6H_2O$ solution with a concentration of 0.05 M was put in a 250 mL conical flask and to it was added 7.5 g of activated hazelnut shell. The mixture was energetically stirred for 1 h. Thereafter, 100 mL of morinda extract obtained by infusing 2 g of morinda in 100 mL was added dropwise into the solution. The whole mixture was then further stirred for 1 h. The impregnated activated hazelnut shell was then washed with an ethanol/water solution. The obtained sample was then treated in a muffle furnace at 200 °C for 2 h at a heating rate of 5 °C per min. After heat treatment, the sample was cooled at room temperature. The obtained metal biochar was named as HN/AC/Fe° (Fig. 1). As generated by the experimental design (DOE), the same procedure was repeated for the different experiments.

Table 1 Experimental variables for the activation of biochar

			Variable level (coded)		
Parameters (factors)	Code	Unit	−1	0	+1
Acid concentration	x_1	N	1	3	5
Hazelnut shell mass	x_2	G	10	15	20
Activation time	x_3	min	30	45	60

Table 2 Experimental variables for the impregnation of iron on activated biochars

			Variable level (coded)		
Parameters (factors)	Code	Unit	−1	0	+1
Iron concentration	x'_1	M	0.005	0.0075	0.01
Morinda mass	x'_2	G	2	6	10
Impregnation time	x'_3	min	60	90	120

2.6. Physicochemical characterizations

A better appreciation of phenomena like adsorption, desorption, and others can be achieved through understanding a material's structural and physicochemical properties. This is the reason why the different biochars were subjected to several characterization techniques.

2.6.1. Fourier transform infrared spectrophotometry (FTIR). Functional groups within the materials along with the vibration, deformation, and the types of interactions within them can be determined using infrared spectrophotometry (IR). Here, the biochars' IR spectra were recorded between 4000 and 400 cm^{-1} using a Nicolet 5700 FTIR instrument (Thermo Electron Corporation).

2.6.2. UV-Vis spectral analysis. A Beckmann Coulter DU 730 Life Science UV-Vis spectrophotometer was used to determine the absorption bands for nZVI. The reduction of metallic Fe^{3+} by morinda stem bark extract was monitored by measuring the UV-Vis spectra. A small aliquot was drawn from the reaction and the spectra of the samples were recorded by scanning the wavelength from 200 nm to 1000 nm.

2.6.3. Thermogravimetric analysis (TGA/TDA). In this analysis, the sample vibration in mass is measured as a function of time for a given temperature profile. Thermal decomposition of the samples was observed using a NETZSCHTG 209F3 instrument (TA Instruments) equipped with platinum sample crucibles. The powder was heated from 50 °C to 1500 °C at a heating rate of 6 °C min^{-1} under a nitrogen atmosphere.

2.6.4. Powder X-ray diffraction (XRD). The amorphous and crystalline structures of the prepared biochars were determined using XRD. This determination make use of dried samples, here, 2 mg of each. The diffraction pattern was recorded on an X-ray powder diffractometer (Bruker D8 Discovery, US) with the Bragg–Bretano two-theta configuration, using CuKα radiation at 27.5 kV and 25 mA. The spectra were obtained in the 2θ range from 6° to 8° with a step of 0.02° and 1 s scan rate.

2.6.5. Scanning electron microscopy. Field emission scanning electron microscopy (FE-SEM) was performed using a JEO JSM 7600F instrument in order to analyze the samples morphology. The sample was coated with a thin layer of gold, then fixed on a metal support and a double-surface carbon strip, and then viewed under 100–5000 magnification at an excitation voltage of 15 kV.

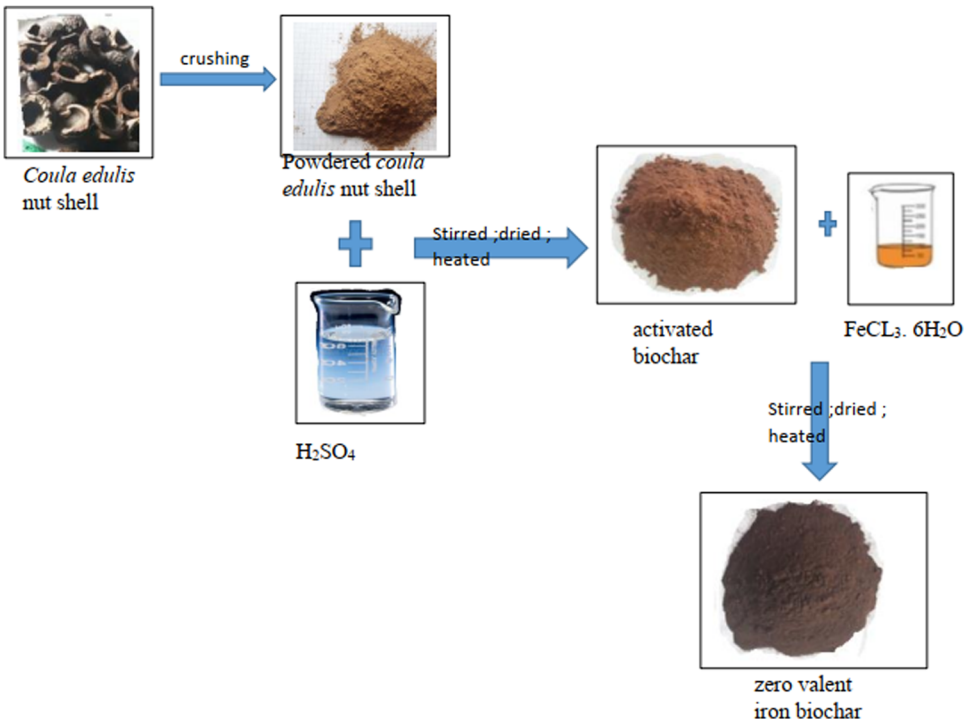

Fig. 1 Schematic of biochar synthesis.

2.6.6 Nitrogen adsorption isotherms and surface area measurements. The total surface areas of the raw material and the prepared biochars were determined using N_2 adsorption isotherms at 77 K in a Quantachrome autosorb AS6AG Station 3 instrument (Institute of Inorganic Chemistry and Structural Chemistry, Dusseldorf University, Germany). The values of the total surface area were calculated from experimental isotherms using the Brunauer–Emmett–Teller (BET) analysis method.

3. Results and discussion

3.1. Experimental design

The experimental matrices with x_1, x_2, x_3 and x'_1, x'_2, x'_3 values along with the experimental and predicted values of the responses Y_1, Y_2, Y_3, and Y_4 are respectively given in Tables 3 and 4. The different parameters' combined effects were investigated statistically. Analysis of variance (ANOVA) for the results of the regression eqn (5)–(8), which represent second-order quadratic equations, was appropriately adapted to the data and results. The quantities of I_2 and MB adsorbed were respectively given by eqn (5) and (6) as a function of the acid concentration (x_1), hazelnut shell mass (x_2), and the activation time (x_3), while eqn (7) and (8) respectively give the amounts of I_2 and MB adsorbed as a function of the iron concentration (x'_1), morinda mass (x'_2), and impregnation time (x'_3). Y_1 and Y_2 respectively represent the I_2 and MB response for activation of the hazelnut shell, while Y_3 and Y_4 represent the I_2 and MB response for the activated hazelnut impregnation with iron using the morinda.

$$Y_1 = 919 - 116.4x_1 - 39.7x_2 - 5.02x_3 + 4.17{x_1}^2 + 0.935{x_2}^2 - 0.049{x_3}^2 - 0.597x_1x_2 + 1.746x_1x_3 + 0.174x_2x_3 \quad (5)$$

$$Y_2 = 3.95 - 6.870x_1 + 1.137x_2 + 0.904x_3 + 0.673{x_1}^2 - 0.020{x_2}^2 - 0.009{x_3}^2 + 0.055x_1x_2 + 0.035x_1x_3 - 0.015x_2x_3 \quad (6)$$

$$Y_3 = 707 - 779x'_1 - 3.3x'_2 - 91.6x'_3 + 18047{x'_1}^2 - 2.444{x'_2}^2 + 6.8{x'_3}^2 + 5.114x'_1x'_2 + 970x'_1x'_3 - 3.20x'_2x'_3 \quad (7)$$

$$Y_4 = 24.03 - 60.80x'_1 - 0.047x'_2 - 1.694x'_3 + 427{x'_1}^2 - 0.001{x'_2}^2 + 0.357{x'_3}^2 0.519x'_1x'_2 + 0.02x'_1x'_3 - 0.015x'_2x'_3 \quad (8)$$

From Tables 3 and 4, it appeared that there was a close similarity between the empirical model responses predicted and those obtained experimentally.

3.1.1. Analysis of variance. The model significance and adequacy were verified using variance analysis in order to study each parameter's influence during preparation of the HN/AC and HN/AC/Fe° samples. Tables 5 and 6 report the results obtained. Generally, the significance of a statistical value for a regression model is determined by a low probability value (p-value).[36] The analysis of variance for the regression model demonstrated that for HN/AC, the factors x_1, ${x_1}^2$, ${x_3}^2$, x_1x_3, and x_2x_3 were significant for the MB response and the factors x_1, x_2, x_3, and x_1x_3 were significant for the I_2 response, while for HN/AC/Fe°, the significant factors were x'_2, x'_3, and ${x'_3}^2$ for the MB response and factors ${x'_2}^2$, $x'_1x'_3$, and $x'_1x'_2$ for I_2 in reference

Table 3 Experimental design matrix for optimization of the parameters using CCD for hazelnut shell activation

				MB (mg g^{-1}), Y_2		IN (mg g^{-1}), Y_1	
Run	H_2SO_4 concentration (x_1)	*Coula edulis* nut shell mass (x_2)	Activation time (x_3)	Exp. value	Pre. value	Exp. value	Pre. value
1	5	20	60	21.681	21.861	226.429	222.601
2	3	15	45	20.919	21.883	220.048	229.140
3	3	15	45	22.509	21.883	221.148	229.140
4	5	10	30	18.489	18.416	230.429	233.044
5	1	10	60	24.084	23.727	243.810	234.906
6	1	20	30	24.650	24.560	350.334	342.268
7	3	20	45	21.008	20.348	203.667	213.117
8	3	15	45	20.675	20.845	219.048	217.895
9	3	15	45	20.178	20.845	220.81	217.895
10	1	15	45	23.965	24.379	258.429	278.031
11	3	15	60	19.148	19.023	172.286	183.412
12	5	15	45	23.384	22.691	203.048	191.136
13	3	15	30	18.962	18.808	233.810	230.374
14	3	10	45	19.954	20.335	271.191	269.431
15	5	10	60	24.476	24.635	253.810	259.954
16	5	20	30	22.974	23.401	126.905	133.887
17	3	15	45	22.896	23.446	220.421	224.369
18	1	10	30	24.993	24.883	406.096	408.002
19	1	20	60	21.752	21.895	216.429	211.892
20	3	15	45	24.614	23.446	222.810	224.369

Exp value = experimental value; pre value = predicted value.

Table 4 Experimental design matrix for optimization of the parameters using CCD for the impregnation of the activated hazelnut shell

				MB (mg g^{-1}), Y_4		IN (mg g^{-1}), Y_3	
Run	Iron concentration (x'_1)	Morinda mass (x'_2)	Impregnation time (x'_3)	Exp. value	Pre. value	Exp. value	Pre. value
1	0.05	10	3	24.781	24.706	130.905	133.306
2	0.075	6	2	24.601	24.606	318.191	254.148
3	0.05	2	1	24.821	24.860	300.191	310.997
4	0.1	2	3	24.336	24.269	218.429	208.802
5	0.1	10	1	24.931	25.027	279.191	279.316
6	0.075	6	2	24.603	24.606	325.810	254.148
7	0.075	6	2	24.662	24.686	315.191	301.179
8	0.1	10	3	24.891	24.876	335.334	327.401
9	0.05	10	1	24.923	25.015	263.81	276.310
10	0.075	6	2	24.814	24.686	320.953	301.179
11	0.1	2	1	24.726	24.825	203.048	203.519
12	0.05	2	3	24.538	24.466	310.572	313.320
13	0.075	10	2	24.197	24.099	304.572	297.479
14	0.075	6	1	24.788	24.462	380.715	356.812
15	0.075	6	2	23.702	23.928	319.191	339.118
16	0.075	2	2	23.797	23.798	306.953	302.555
17	0.075	6	2	23.863	23.928	324.572	339.118
18	0.075	6	3	23.880	24.109	322.572	334.984
19	0.05	6	2	23.651	23.668	380.715	352.260
20	0.1	6	2	23.769	23.655	331.572	348.536

Exp value = experimental value; pre value = predicted value.

to *p*-values $\leq$00.5 and the higher *f*-ratios.[37] Based on the methodology used, a correlation coefficient $\geq$0.75 or 75% confirms the validity of the model. In the present work, the values were 93.74% and 95.80% respectively for MB and I_2 for HN/AC, and 92.75% and 95.41% respectively for MB and I_2 for HN/AC/Fe°, thus indicating the good correlation among the various factors investigated and the experimental data, which confirmed the prediction.

Fig. 2 and 3 show the experimental values *versus* predicted values for the MB and iodine indices, respectively. It could be observed that the predicted values obtained were quite close to the experimental values, indicating that the models developed were successful in capturing the correlation between the biochars; preparation variables to the MB and iodine indices.

3.1.2. Response surface, Pareto diagram, and main effects of the factors on the methylene blue number and iodine number. The Pareto diagram, the three surface response, and the various parameters influences are shown in Fig. 4. This figure helps the establishment of a connection among the interactions between the parameters taken into account during the different biochar preparation. The synergistic effect of the investigated factors makes it possible to observe the methylene

Table 5 Analysis of variance of Y for HN/AC

		Y_2			Y_1		
Source	df	Mean square	F-value	p-value	Mean square	F-value	p-value
x_1	1	7.120	11.070	0.010*	18 877.030	145.080	<0.0001*
x_2	1	0.0005	0.0007	0.979	7928.280	60.930	<0.0001*
x_3	1	0.115	0.179	0.683	5513.570	42.370	0.0002*
x_1x_2	1	2.380	3.700	0.091	285.150	2.190	0.177
x_1x_2	1	9.030	14.040	0.006*	21 955.180	168.730	<0.0001*
x_2x_3	1	10.740	16.700	0.004*	1365.660	10.500	0.012
x_1^2	1	19.430	30.200	0.0006*	910.330	3.660	0.063
x_2^2	1	0.680	1.060	0.334	1691.930	2.210	0.176
x_3^2	1	9.990	15.530	0.004*	230.900	1.770	0.219

For Y_1, R_2 = 95.50%; for Y_2, R_2 = 93.99.

Table 6 Analysis of variance of Y for HN/AC/Fe°

		Y_4			Y_3		
Source	df	Mean square	F-value	p-value	Mean square	F-value	p-value
x_1'	1	0.0004	0.010	0.923	34.670	0.048	0.833
x_2'	1	0.227	6.060	0.039*	64.420	0.088	0.774
x_3'	1	0.311	8.320	0.020*	1191.220	1.630	0.237
$x_1'x_2'$	1	0.022	0.576	0.469	20 919.940	28.680	0.0007*
$x_1'x_3'$	1	3.125×10^{-6}	0.0001	0.993	4706.830	6.450	0.035*
$x_2'x_3'$	1	0.030	0.806	0.396	1313.900	1.800	0.216
$x_1'^2$	1	0.191	5.120	0.054	3.320	0.005	0.948
$x_2'^2$	1	0.001	0.029	0.869	7117.400	9.760	0.014*
$x_3'^2$	1	0.342	9.150	0.0164*	84.55	0.116	0.742

For Y_3, R_2 = 95.41%; for Y_4, R_2 = 92.75%. *Significant factors; df = degree of freedom.

blue and iodine number variation for each of the samples. From the three-dimensional response surface for HN/AC, Fig. 4(a) shows that the MB number decreased with the increase in HN mass and increase in activation time, while Fig. 4(b) reveals that the iodine number decreased when the activation decreased and the HN mass increased. For HN/AC/Fe°, Fig. 4(c) shows that the methylene blue number increased as a result of the decrease in morinda mass and impregnation time, while the iodine number increased with the increase in morinda mass and decrease in impregnation time. This was observed at constant concentrations of the activation and impregnation agents. It was also revealed from the various standard effects (greater than 2.306) acquired *via* the Pareto diagram that the interaction of the different factors had a more prominent effect compared to the effect of the single factors alone.

3.1.3. Optimal synthesis conditions. The optimum conditions for the preparation of the biochars were obtained at the end of the optimization process. The optimal conditions were as follow: sulphuric acid concentration was 1 N for a HN mass of 10 g and activation time of 30 min for HN/AC preparation; in regards to HN/AC/Fe°, the optimal conditions were: iron concentration 0.075 M for a morinda mass of 6 g and an impregnation time of 60 min. The MB and iodine number values for these optimal conditions were, respectively, 24.99 and 406.096 mg g^{-1} for HN/AC, and 24.788 and 380.715 mg g^{-1} for HC/AC/Fe°. The biochars obtained under these optimal conditions were characterized with a view to confirm their properties.

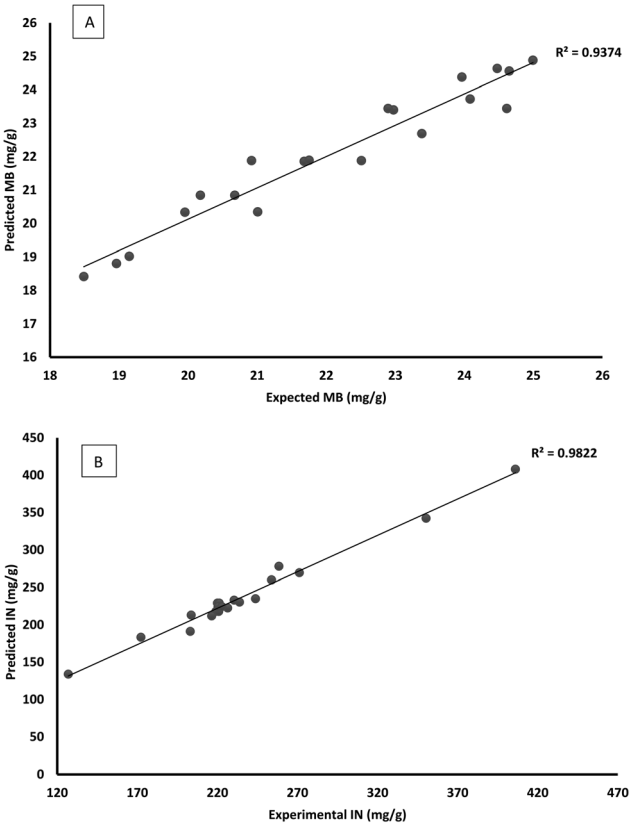

Fig. 2 Predicted *vs.* experimental methylene blue index for HN/AC (A). Predicted *vs.* experimental iodine number index for HN/AC.

3.2. Functional groups analysis by FTIR

The vibrational bands of the different materials were recorded between 4000 and 400 cm^{-1} and are shown in the FTIR spectra in Fig. 5. The following bands were recorded for the powdered hazelnut shell: the first one between 3500 and 3400 cm^{-1}, which was intense and corresponded to the elongation vibrations of the O–H bond of water molecules.[38] Also, C–H aliphatic CH_2 bonds stretching vibrations were observed at 2935.42 cm^{-1},[39] while another band around 1741.58 cm^{-1} was attributed to the deformation vibrations of C═C bonds of aromatic rings. The band observed at about 1618.14 cm^{-1} could be assigned to the carbonyl (C═O) stretching vibration of amide linkage and stretching vibration of C–N of aromatic amines[40] The band around 1513.99 cm^{-1} was assigned to the OH bending vibrational mode due to the adsorption of moisture when the FTIR sample discs were prepared.[41] The weak band at about 1461.92 cm^{-1} corresponded to the C═C bond stretching of an ethane group. Another feeble band was observed at about 1242.07 cm^{-1}, which could be assigned to C–O stretching. The band found around 1031.83 cm^{-1} might be ascribed to C–OH bond stretching.[42] Finally, the band observed around 605.59 cm^{-1} could be ascribed to the C–O–C elongation vibrations band from cellulose.[43] Comparing the

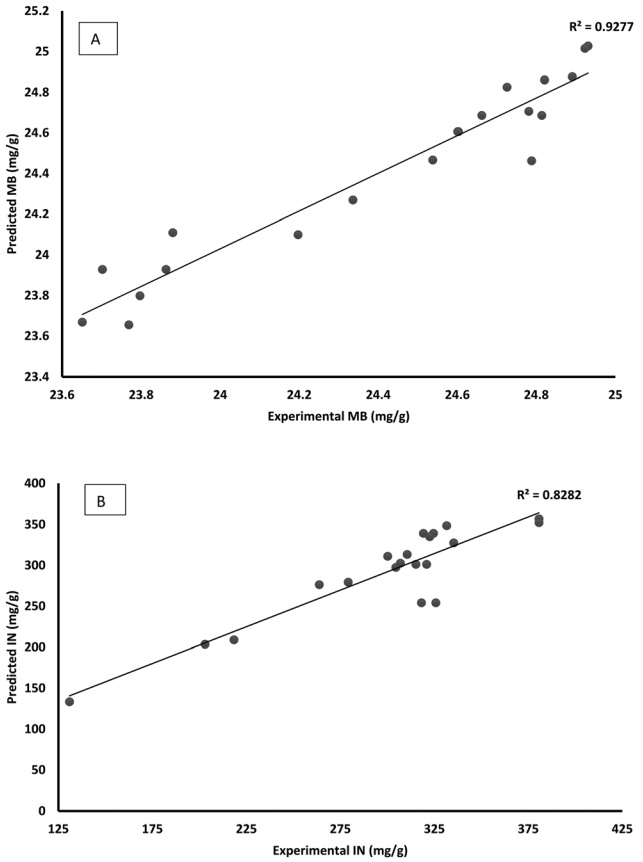

Fig. 3 Predicted *vs.* experimental methylene blue index for HN/AC/Fe° (A). Predicted *vs.* experimental iodine number index for HN/AC/Fe° (B).

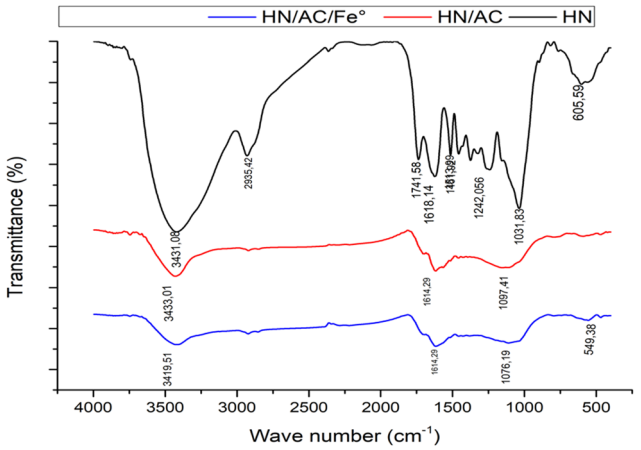

Fig. 5 Superimposed IR spectra of HN, HN/AC, and HN/AC/Fe°.

spectrum of the precursor (HN) with those of the prepared biochars (HN/AC and HN/AC/Fe°), a decrease in intensity in the bands around 3400 cm^{-1} could be observed, while no bands were observed between 3400 and 1741.58 cm^{-1}, an indication that the material activation and heating led to the decomposition of certain surface chemical functional groups, like oxygenated hydrocarbons, which reflect the carbohydrate structures of cellulose and hemicellulose.[44] In addition, a small shift from 605.59 cm^{-1} to 549.38 cm^{-1} was observed in the HN/AC/Fe° FTIR spectrum, which was due to the Fe–O stretching vibrations.

3.3. UV-Vis spectral analysis

UV-Vis spectral analysis allowed us to highlight the reduction of Fe^{3+} to nZVI. This was confirmed by the sudden change in the

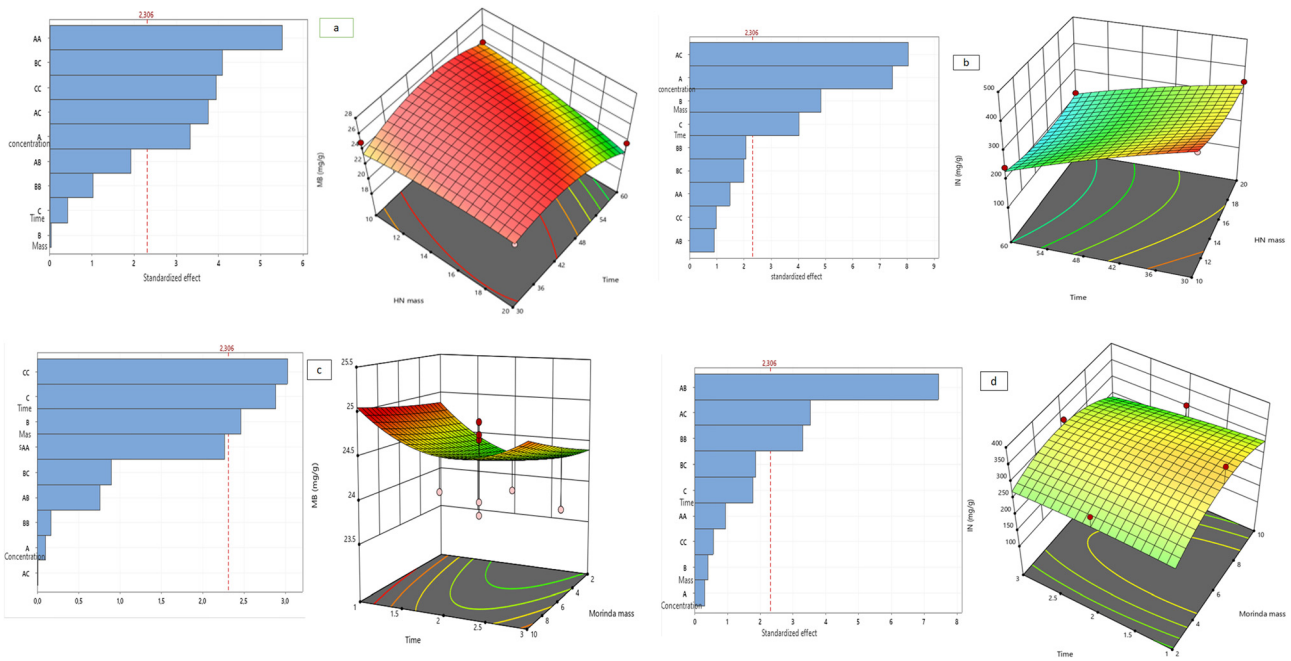

Fig. 4 Pareto diagrams associated with the three-dimensional response surfaces: MB for HN/AC (a), IN for HN/AC (b), MB for HN/AC/Fe° (c), and IN for HN/AC/Fe° (d).

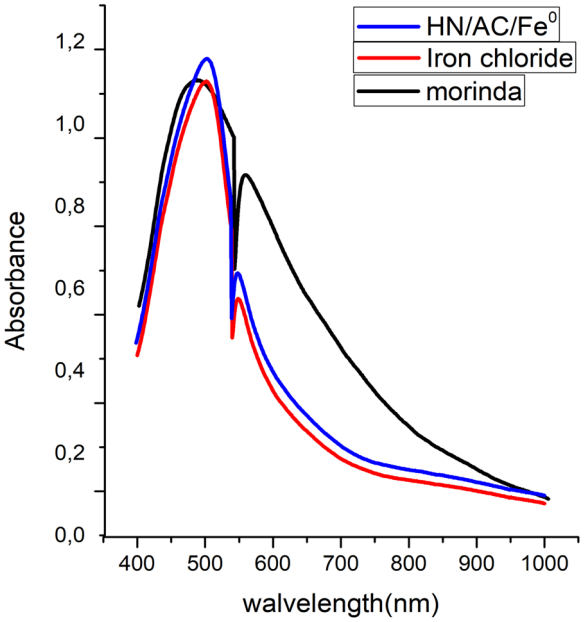

Fig. 6 UV-Visible absorption spectra of morinda stem bark extract, aqueous solution of Fe^{3+} ions, and the synthesized nZVI.

visible colour of the reaction medium, serving as a preliminary indicator of the formation of nZVI. In the present study, an immediate change in the colour of the solution from reddish-brown to black was observed after the addition of morinda extract, indicating the rapid synthesis of nZVI;[45] allowing us to conclude that the formation of the dark colour of the synthesized nZVI was essentially due to the complexation of Fe^{3+} with the phenolic group in the plant extract as a metal–ligand interaction between Fe^0 and the polyphenolic compound *via* the C═O bond.[31] The UV-Vis spectra of the aqueous Fe^{3+} ions solution, morinda stem bark extract, and synthesized HN/AC/Fe° (Fig. 6) proved that the absorption spectrum of nZVI exhibited maximum absorption in the range of 420–510 nm, which was consistent with the characteristic absorption peak for metallic iron previously reported.[46]

3.4. XRD analysis

Fig. 7 reveals the precursor and biochars mineralogical phase variation through XRD analysis. The diffraction pattern of the precursor HN showed a dome between 18° and 23° also, with no peaks observed, reflecting the material's crystallinity. This monitoring confirmed the precursor's amorphous nature, leading to the sample's porous nature, which benefits chemical adsorption. Thus, HN is a good precursor for biochar preparation. Comparing the diffractogram of the precursor to that of the prepared biochars, peaks were observed at 20.8° and 21.1°, respectively, on HN/AC and HN/AC/Fe°, which were related to the crystallographic plane of cellulose. Sharp and intense peaks at 25.38° and 26.67° in the HN/AC diffractogram and 26.73° for HN/AC/Fe°, resulted from the crystalline size enlargement and further development of pores.[47] Peaks at 2θ = 35.95° and 63.22° in HN/AC/Fe° confirmed the presence of iron zero-valent particles.[30] These experimental results reveal that morinda stem bark extract

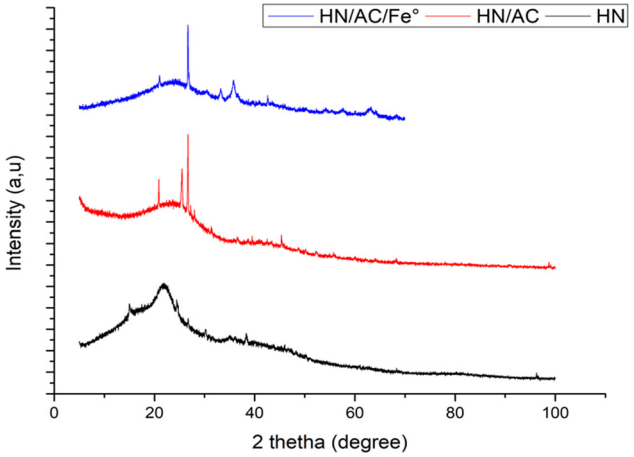

Fig. 7 X-ray diffraction patterns of HN, HN/AC and HN/AC/Fe°.

could act as an efficient reducing agent and stabilizing agent in the reduction of ferric iron into zero-valent iron.

3.5. Scanning electron microscopy (SEM)

Fig. 8 shows the micrographs of HN, HN/AC, and HN/AC/Fe°. Comparing the microstructure of HN (Fig. 8(a)) to that of HN/AC (Fig. 8(b)), it could be observed that HN/AC had a higher porosity than HN. This was a result of the chemical and physical activation of HN/AC, which led to a decomposition of the organic matter that obstructed the pores. Comparing side by side the microstructure of HN/AC/Fe° (Fig. 8(c)) with that of HN and HN/AC, it could be noticed that HN/AC/Fe° had the highest porosity. This was a consequence of the impregnation of iron on the matrix and the physical activation, which increased the porosity and surface functional groups.

3.6. Nitrogen adsorption isotherms and surface area measurements

Table 7 shows the specific surface areas of the different samples. It can be seen that the HN/AC material had a specific surface area 50 times greater than that of the HN sample, while the HN/AC material had a specific surface area 2 times greater than that of the HN/AC sample. The increase in specific surface area observed was due to the chemical activation, impregnation, and carbonization, which resulted in a change in the textural properties. These properties corroborate the results in Section 3.4 and will play a decisive role in the process of sequestering water pollutants.

3.7. Thermogravimetric analysis (TGA)

Thermal decomposition of the HN/AC and HN/AC/Fe° samples was investigated, and the results are given in Fig. 9. HN/AC and HN/AC/Fe° both showed a progressive loss of mass of about 5.47% and 4.18%, respectively, in the range of 100–200 °C. This could be ascribed to the evaporation of the adsorbed water coupled with the volatilization of hydrocarbons. The second large mass loss of about 67.98% and 42.32%, respectively, for HN/AC and HN/AC/Fe° happened between 300 °C and 800 °C, and resulted from the decomposition of organic matter. This

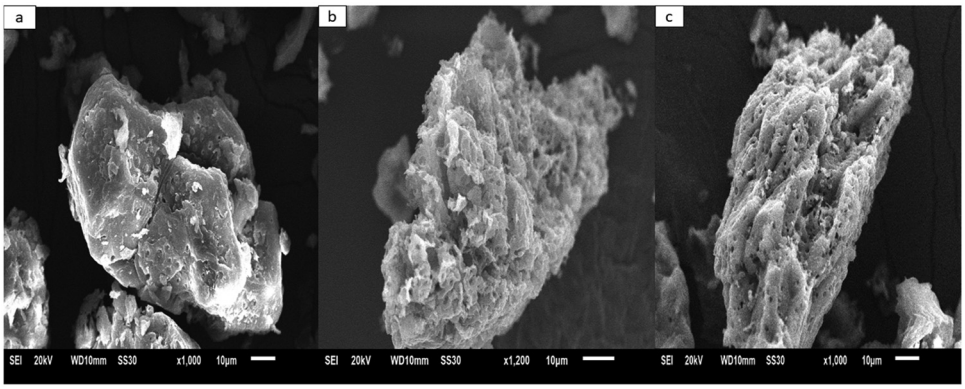

Fig. 8 Scanning electron microscopy images of HN (a), HN/AC (b) and HN/AC/Fe° (c).

Table 7 Specific surface areas of the samples

Adsorbent	HN	HN/AC	HN/AC/Fe
Specific surface area ($m^2\ g^{-1}$)	3.640	178.136	361.750

occurrence was ascribed to an auto-catalytic reaction, which could have caused the precursor diminution and continuous melting. The second loss in mass observed for the pair of sample corresponded to the cellulose, hemicellulose and lignin progressive decomposition.

3.8. Efficiency tests for the prepared biochars

The efficiency of HN, HN/AC, and HN/AC/Fe° for adsorbing malachite green was tested. This was done by putting in contact 0.1 g of each adsorbents with 50 mL of 100 mg L^{-1} malachite green and then stirring for 50 min. It could be observed from Fig. 10 that the removal percentage of the biochar increased as a function of the activation and impregnation, respectively, as 20.23% for HN, 30.35% for HN/AC, and 97.08% for HN/AC/Fe°. The great ability of HN/AC/Fe° to eliminate malachite green was a result of its more significant textural properties.

In order to better understand the adsorption mechanism of malachite green onto the raw material and prepared biochars, Langmuir and Freundlich isotherms were considered, respectively, according to eqn (9) and (10).[31] The Langmuir isotherm stipulates monolayer adsorption on homogeneous and energetically equivalent active sites, while the Freundlich isotherm is an empirical model for predicting multilayer adsorption mechanisms on heterogeneous active sites and so is applied to multilayer adsorption.

$$\frac{C_e}{q_e} = \frac{1}{K_L q_{max}} + \frac{1}{q_{max}} C_e \quad (9)$$

$$R_L = \frac{1}{K_L C_0} \quad (10)$$

$$q_e = K_f C_e^{1/n} \quad (11)$$

The different parameters corresponding to these isotherms are listed in Table 8.

With regard to Fig. 11(a) and (b) and the results given in Table 8, the Langmuir model was adequate to describe the adsorption of malachite green onto HN/AC and HN/AC/Fe° because of their correlation coefficients (R^2), which converge to unity, and their small error functions (χ^2). The numerical values of the parameter R_L indicated that the adsorption was

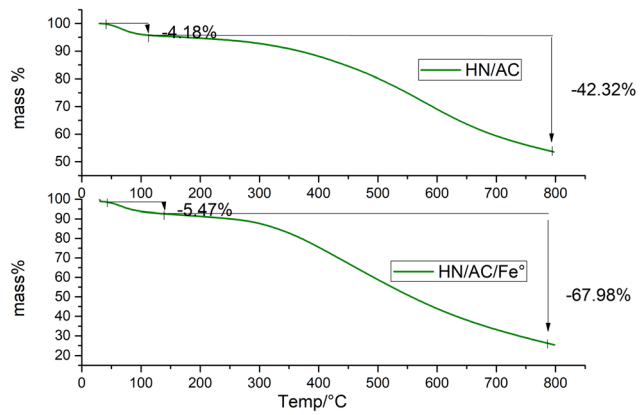

Fig. 9 Thermogravimetric analysis curves for HN/AC and HN/AC/Fe°.

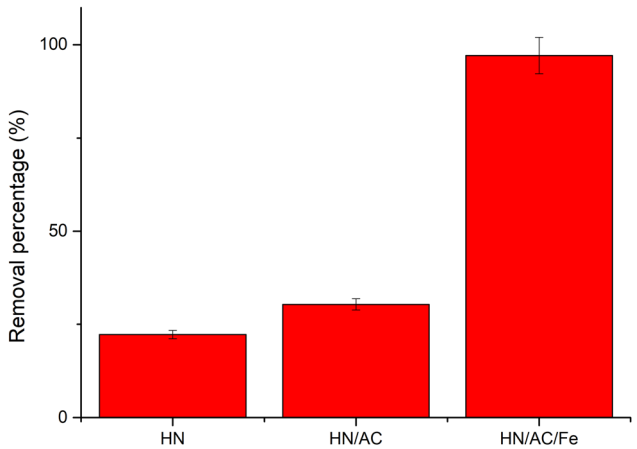

Fig. 10 Malachite green removal percentage as a function of the adsorbents.

Table 8 Isotherms parameters for HN, HN/AC, and HN/AC/Fe°

	Parameter	HN	HN/AC	HN/AC/Fe°
Langmuir	Q_{max}	18.484	15.290	11.148
	K_L	10.820	1.630	4.505
	K_a	199.999	24.923	50.220
	R_L	0.001	0.006	0.002
	R^2	0.393	0.967	0.994
	χ^2	63.006	39.910	45.743
Freundlich	K_F	6.199	22.175	53.303
	$1/n$	−0.161	0.101	−0.219
	R^2	0.092	0.027	0.574
	χ^2	90.491	65.846	57.035

irreversible and as such, the adsorbents/adsorbate interactions were chemical. Furthermore, the Langmuir isotherm revealed that the adsorption of malachite green on the surface of HN/AC and HN/AC/Fe° occurred as a monolayer at the homogeneous sites. The apparent equilibrium constant (K_a), a product of Q_{max} and K_L derived from the Langmuir isotherm, was considered as a measure of the relative affinity of the biochars towards malachite green. The K_a values (Table 8) indicate that HN/AC/Fe° had an affinity to fix malachite green two times greater than HN/AC. This was supported by the SEM results, which showed that HN/AC/Fe° had a higher porosity than HN/AC. Also, the FTIR data showed new functional groups in HN/AC/Fe° that could induce increased affinity.

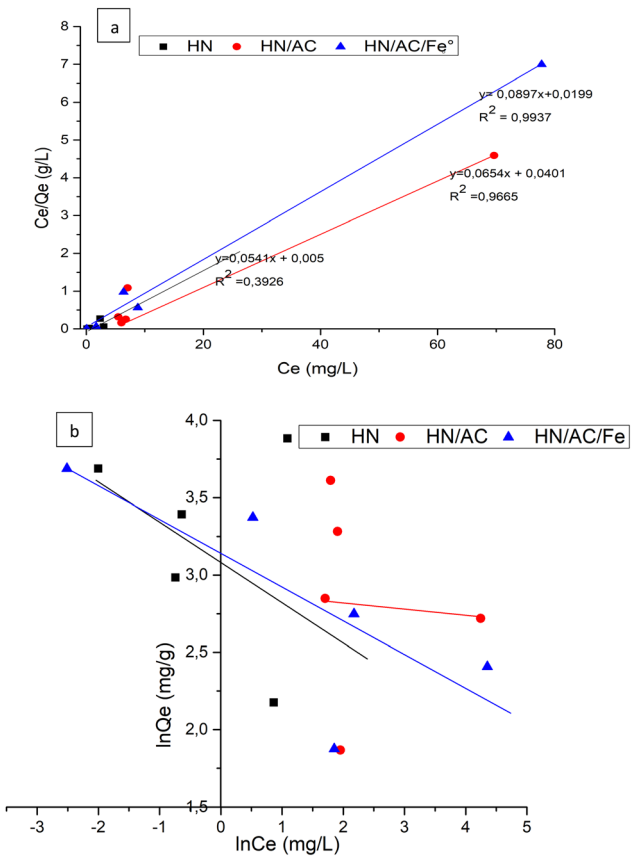

Fig. 11 Langmuir adsorption isotherms for the removal of malachite green using HN, HN/AC, and HN/AC/Fe° (a). Freundlich adsorption isotherms for the removal of malachite green using HN, HN/AC, and HN/AC/Fe° (b).

4. Conclusion

African hazelnut shell-activated biochar was used to prepare an eco-friendly engineered biochar with nZVI. In an impartial and unbiased manner, it was found that the optimization of three factors could to a great extent influence the properties of the biochar. With regard to the activated biochar HN/AC, the optimum conditions were H_2SO_4 concentration of 1 N, HN mass of 10 g, and activation time of 30 min. For HN/AC/Fe°, the optimal conditions were an iron concentration of 0.075 M, morinda mass of 6 g, and an impregnation time of 1 h. For this cause, response surface methodology, involving a mathematical model, was used. Designed Expert vision 13 software was used and the factors investigated. The expected responses was the methylene blue index and iodine number index, and each time, the expected values observed were close to the predicted values obtained. Considering the above-mentioned factors in the experimental model led to the optimal conditions. The experimental responses obtained under these conditions for both biochars were within an error range much less than 5% of that predicted. The chemical and physical activation and impregnation led to the formation of new functional groups on the surfaces of both samples. The microstructure analysis revealed that these processes increased the porosity of each char. Hence, African hazelnut shell and morinda stem bark extract could be used for the synthesis of economic and eco-friendly iron biochars.

Data availability

The data that support the findings of this study are available in the main text, as well as from the corresponding authors upon reasonable request.

Conflicts of interest

The authors declare no conflicts of interests.

Acknowledgements

This study was financed by the own resources of the different authors.

References

1 T. Tiegam, R. Fregue, I. Ionel and N. Adina, Optimization of the activated carbon synthesis of peanut shells, in 27th European biomass conference and exhibition, 27-30 May 2019, Lisbon, Portugal, 2019, no. July, pp. 1849–1855. doi: 10.5071/27thEUBCE2019-5BV.3.29.

2 N. Sahu and S. Shukla, Adsorptive removal of Arsenic(III) from magnetic biochar fabricated from agricultural waste biomass, *J. Appl. Sci. Innov. Technol.*, 2022, **1**(2), 52–55.

3 S. M. Kharrazi, N. Mirghaffari, M. M. Dastgerdi and M. Soleimani, A novel post-modification of powdered activated carbon prepared from lignocellulosic waste through thermal tension treatment to enhance the porosity and

heavy metals adsorption, *Powder Technol.*, 2020, **366**, 358–368, DOI: 10.1016/j.powtec.2020.01.065.

4 Y. Guo and D. A. Rockstraw, Physicochemical properties of carbons prepared from pecan shell by phosphoric acid activation, *Bioresour. Technol.*, 2007, **98**, 1513–1521, DOI: 10.1016/j.biortech.2006.06.027.

5 A. H. Basta, V. Fierro, H. Saied and A. Celzard, Effect of deashing rice straws on their derived activated carbons produced by phosphoric acid activation, *Biomass Bioenergy*, 2011, **35**(5), 1954–1959, DOI: 10.1016/j.biombioe.2011.01.043.

6 C. D. Atemkeng, *et al.*, Chemical preparation and physicochemical characterization of powdered activated carbons based on safou (Dacryodes edulis) seeds, *J. Mater. Environ. Sci.*, 2020, **2020**(6), 896–910, [Online]. Available: https://www.jmaterenvironsci.com.

7 S. Das, A. Pal and A. Debnath, Polyaniline – coated magnesium ferrite nanocomposite: synthesis, characterization, fabrication cost analysis and dye sorption behavior with scale – up design, *ChemistrySelect*, 2023, **8**(29), e202300928.

8 A. Deb, S. Das and A. Debnath, Fabrication and characterization of organometallic nanocomposite for efficient abatement of dye laden wastewater: CCD optimization, adsorption mechanism, co-existing ions, and cost analysis, *Chem. Phys. Lett.*, 2023, **830**, 140820, DOI: 10.1016/j.cplett.2023.140820.

9 M. Zue Mve, R. Kouya Biboutou, F. Eba and D. Njopwouo, Kinetic and Isotherm Studies of Al(III) Ions Removal from Aqueous Solution by Adsorption onto Coula edulis Nut Shell Activated Carbon, *J. Environ. Earth Sci.*, 2016, **6**(5), 37–47.

10 C. Zhao, B. Wang, B. K. G. Theng, P. Wu, F. Liu, S. Wang, X. Lee, M. Chen, L. Li and X. Zhang, Science of the Total Environment Formation and mechanisms of nano-metal oxide-biochar composites for pollutants removal: A review, *Sci. Total Environ.*, 2021, **767**, 145305, DOI: 10.1016/j.scitotenv.2021.145305.

11 L. Liang, F. Xi, W. Tan, X. Meng, B. Hu and X. Wang, Review of organic and inorganic pollutants removal by biochar and biochar – based composites, *Biochar*, 2021, **3**(3), 255–281, DOI: 10.1007/s42773-021-00101-6.

12 S. Arivoli, M. Hema and P. M. D. Prasath, Adsorption of malachite green onto carbon prepared from borassus bark adsorption of malachite green onto carbon prepared from, *Sci. Eng.*, 2009, **34**(2), 31–42.

13 L. Verma and J. Singh, As(III) removal using engineered biochar synthesized from waste biomass of a Timber plant refuse, *J. Appl. Sci. Innov. Technol.*, 2022, **1**(1), 6–9.

14 L. Verma, N. Kanaujia and J. Singh, A review on Arsenic remediation from the water by biochar developed from the different waste biomasses Journal of Applied Science, Innovation & Technology (JASIT) A review on Arsenic remediation from the water by biochar developed from the different wa, *J. Appl. Sci. Innov. Technol.*, 2023, **2**, 1–10.

15 Y. Ma, W. Liu, N. Zhang, Y. Li, H. Jiang and G. Sheng, Polyethylenimine modified biochar adsorbent for hexavalent chromium removal from the aqueous solution, *Bioresour. Technol.*, 2014, **169**, 403–408, DOI: 10.1016/j.biortech.2014.07.014.

16 A. Mohseni-Bandpi, B. Kakavandi, R. R. Kalantary, A. Azari and A. Keramati, Development of a novel magnetite-chitosan composite for the removal of fluoride from drinking water: Adsorption modeling and optimization, *RSC Adv.*, 2015, **5**, 73279–73289.

17 K. S. R. Yingwen Xue, B. Gao, Y. Yao, M. Inyang, M. Zhang and A. R. Zimmerman, Hydrogen peroxide modification enhances the ability of biochar (hydrochar) produced from hydrothermal carbonization of peanut hull to remove aqueous heavy metals: Batch and column tests, *Chem. Eng. J.*, 2012, **200–2012**, 673–680, DOI: 10.1016/j.cej.2012.06.116.

18 L. Wang, J. Rinklebe, Y. Sik, O. Daniel and C. W. T. Daniel, Biochar composites: Emerging trends, field successes and sustainability implications, *Soil Use Manage.*, 2021, **38**(1), 14–38, DOI: 10.1111/sum.12731.

19 E. Issaka, *et al.*, Chemosphere Biochar-based composites for remediation of polluted wastewater and soil environments: Challenges and prospects, *Chemosphere*, 2022, **297**, 134163, DOI: 10.1016/j.chemosphere.2022.134163.

20 S. Machado, W. Stawi, P. Slonina, A. R. Pinto, J. P. Grosso and H. P. A. Nouws, Application of green zero-valent iron nanoparticles to the remediation of soils contaminated with ibuprofen, *Sci. Total Environ.*, 2013, **461–462**, 323–329.

21 T. Huang, V. Bhat, C. Carlson and M. Technology, *US Pat.*, 2, 12, 2015.

22 W. Liu, *et al.*, Adsorption of Pb^{2+}, Cd^{2+}, Cu^{2+}, and Cr^{3+} onto titanqte nanotubes: Coöpetition and effect of inorganic ions, *Sci. Total Environ.*, 2013, **456–457**, 171–180, DOI: 10.1016/j.scitotenv.2013.03.082.

23 R. Prasad, V. Kumar and K. S. Prasad, Nanotechnology in sustainable agriculture: Present concerns and future aspects, *Afr. J. Biotechnol.*, 2014, **13**(6), 705–713, DOI: 10.5897/AJBX2013.13554.

24 F. Zhu, S. He and T. Liu, Effect of pH, temperature and co-existing anions on the Removal of Cr(VI) in groundwater by green synthesized nZVI/Ni, *Ecotoxicol. Environ. Saf.*, 2018, **163**, 544–550, DOI: 10.1016/j.ecoenv.2018.07.082.

25 T. Li, *et al.*, Simultaneous removal of *p*-nitrophenol and Cr(VI) using biochar supported green synthetic nano zero valent iron-copper: Mechanistic insights and toxicity evaluation, *Process Saf. Environ. Prot.*, 2022, **167**, 629–640, DOI: 10.1016/j.psep.2022.09.049.

26 A. Soliemanzadeh and M. Fekri, The application of green tea extract to prepare bentonite-supported nanoscale zero-valent iron and its performance on removal of Cr(VI): Effect of relative parameters and soil experiments, *Microporous Mesoporous Mater.*, 2017, **239**(VI), 60–69, DOI: 10.1016/j.micromeso.2016.09.050.

27 M. Mystrioti, C. Sparis, D. Papasiopi, N. Xenidis, A. Dermatas and D. Chrysochoou, Assessment of polyphenol coated nano zero valent iron for hexavalent chromium removal from contaminated waters, *Bull. Environ. Contam. Toxicol.*, 2015, **3**(2), 54–67, [Online]. Available: https://repositorio.unan.edu.ni/2986/1/5624.pdf.

28 R. K. Chrysochoou, Reduction of hexavalent chromium by green tea polyphenols and green tea nano zero-valent iron (GT-nZVI), *Bull. Environ. Contam. Toxicol.*, 2017, **98**(3), 2017.

29 I. A. W. Tan, A. L. Ahmad and B. H. Hameed, Optimization of preparation conditions for activated carbons from coconut husk using response surface methodology, *Chem. Eng. J.*, 2008, **137**, 462–470, DOI: **10.1016/j.cej.2007.04.031**.

30 M. Ahmad, A. R. A. Usman, M. I. Rafique and M. I. Al-wabel, Engineered biochar composites with zeolite, silica, and nano-zerovalent iron for the efficient scavenging of chlortetracycline from aqueous solutions, *Environ. Sci. Pollut. Res.*, 2019, **26**, 15136–15152.

31 J. Nga, J. Avom, J. Tonga Limbe, D. Ndinteh, H. L. Assonfack and C. M. Kede, Kinetics and Thermodynamics of β -Carotene Adsorption onto Acid-Activated Clays Modified by Zero Valent Iron, *J. Chem*, 2022, **2022**, 17–19, DOI: **10.1155/2022/6505556**.

32 S. Mandal, S. Pu, S. Adhikari, H. Ma and D. Kim, Technology Progress and future prospects in biochar composites: Application and reflection in the soil environment, *Crit. Rev. Environ. Sci. Technol.*, 2020, 1–53, DOI: **10.1080/10643389.2020.1713030**.

33 M. Saban Tanyildize, Modeling of adsorption isotherms and kinetics of reactive dye from aqueous solution by peanut hull, *Chem. Eng. J.*, 2011, **168**, 1234–1240, DOI: **10.1016/j.cej.2011.02.021**.

34 E. P. Box, J. Stuart Hunter and W. G. Hunter, Statistics for Experimenters, An introduction to Design, Data Analysis, and Model Building. 1984.

35 C. Aurelle, *et al.*, Removal of methylene blue by African hazelnut shell modified by zero valent iron and silver bimetallic nanoparticles, 2020, **2**(1), 46–56.

36 S. S. K. M. Meera, S. Begum, Á. Ccd, Á. C. Vi and Á. Adsorption, *Optimization using central composite design (CCD) for the biosorption of Cr(VI) ions by cross linked chitosan carbonized rice husk (CCACR)*, 2013, pp. 293–302, DOI: **10.1007/s10098-012-0512-3**.

37 J. N. Sahu, J. Acharya and B. C. Meikap, Bioresource Technology Optimization of production conditions for activated carbons from Tamarind wood by zinc chloride using response surface methodology, *Bioresour. Technol.*, 2010, **101**(6), 1974–1982, DOI: **10.1016/j.biortech.2009.10.031**.

38 A. A. Babaei, A. Azari, R. R. Kalantary and B. Kakavandi, Enhanced removal of nitrate from water using nZVI @ MWCNTs composite: synthesis, kinetics and mechanism of reduction, *Water Sci. Technol.*, 2015, **72**(11), 1889–2102, DOI: **10.2166/wst.2015.417**.

39 A. D. Dwivedi and K. Gopal, Colloids and Surfaces A: Physicochemical and Engineering Aspects Biosynthesis of silver and gold nanoparticles using Chenopodium album leaf extract, *Colloids Surf., A*, 2010, **369**(1–3), 27–33, DOI: **10.1016/j.colsurfa.2010.07.020**.

40 C. Jayaseelan, R. Ramkumar, A. Abdul and P. Perumal, Green synthesis of gold nanoparticles using seed aqueous extract of Abelmoschus esculentus and its antifungal activity, *Ind. Crop. Prod.*, 2013, **45**, 423–429, DOI: **10.1016/j.indcrop.2012.12.019**.

41 V. A. Online, B. Kakavandi, R. R. Kalantary, A. Azari and A. Keramati, Development of a novel magnetite-chitosan composite for the removal of fluoride from drinking water: Adsorption modeling and optimization Anoushiravan, *R. Soc. Chem.*, 2015, 1–29, DOI: **10.1039/C5RA11294J**.

42 D. H. K. Reddy and S. Lee, Application of magnetic chitosan composites for the removal of toxic metal and dyes from aqueous solutions, *Adv. Colloid Interface Sci.*, 2013, **201–202**, 68–93, DOI: **10.1016/j.cis.2013.10.002**.

43 A. L. Ortiz, Influence of preparation conditions in the textural and chemical properties of activated carbons from a novel biomass precursor: The coffee endocarp, *Bioresour. Technol.*, 2008, **99**, 7224–7231, DOI: **10.1016/j.biortech.2007.12.068**.

44 N. S. Nasri, H. Basri and A. Garba, Synthesis and characterization of low-cost porous carbon from palm oil shell via K_2CO_3 chemical activation process, *Technol. Eng. Rev. Res. Adv. I*, 2015, **735**, 36–40, DOI: **10.4028/www.scientific.net/AMM.735.36**.

45 A. M. Abdelfatah, M. Fawzy, A. S. Eltaweil and M. E. El-Khouly, Green Synthesis of Nano-Zero-Valent Iron Using Ricinus Communis Seeds Extract: Characterization and Application in the Treatment of Methylene Blue-Polluted Water, *ACS Omega*, 2021, **6**(39), 25397–25411, DOI: **10.1021/acsomega.1c03355**.

46 A. O. Dada, F. Adekola and E. Odebunmi, Investigation of the Synthesis and Characterization of Manganese, no. January 2018, 2014.

47 E. Workie, Y. Mengist, M. Sisay and A. Ma, Preparation, characterization and cost analysis of activated biochar and hydrochar derived from agricultural waste: a comparative study, *SN Appl. Sci*, 2019, **1**(8), 1–8, DOI: **10.1007/s42452-019-0936-z**.